Available online at www.CivileJournal.org

Civil Engineering Journal

(E-ISSN: 2476-3055; ISSN: 2676-6957)

Vol. 12, No. 05, May, 2026

Characteristics of Liquefaction in Embankment Models Reinforced with Hybrid Piles

Muhammad Yunus [1*], Achmad B. Muhiddin [1], Tri Harianto [1], Ardy Arsyad [1]

[1] *Department of Civil Engineering, Faculty of Engineering, Hasanuddin University, Gowa 92172, Indonesia.*

Received 10 December 2025; Revised 20 March 2026; Accepted 04 April 2026; Published 01 May 2026

Abstract

Liquefaction of saturated loose sand poses a serious threat to the stability of embankments subjected to seismic loading. This study aims to evaluate the effectiveness of an innovative and environmentally friendly liquefaction mitigation technique using hybrid piles (HPs) that combine structural stiffness and vertical drainage functions. A series of 1-g shaking table tests was conducted on embankment models constructed over saturated sand with an initial relative density of 40%. The models were subjected to repeated sinusoidal seismic excitations with peak ground accelerations (PGA) ranging from 0.3 g to 0.5 g. The performance of the HPs system was assessed by analyzing cone penetration resistance, acceleration response, excess pore water pressure ratio, changes in relative density and void ratio, and surface settlement. The experimental results demonstrate that the HPs system significantly enhances soil densification and stiffness, as indicated by a 1.3–3.0-fold increase in penetration resistance and a relative density increase of up to 7–10% in deeper layers. The HPs system reduced the maximum excess pore water pressure ratio by up to 16.26%, thereby delaying liquefaction onset and enhancing pore pressure dissipation under repeated seismic loading. In addition, settlement was reduced by approximately 37–42% compared with the unreinforced model across all PGA levels. The novelty of this study lies in the integrated use of locally sourced timber and prefabricated vertical drains within a single reinforcement element, providing combined mechanical reinforcement and drainage enhancement. These findings confirm that HPs offer a sustainable and effective solution for mitigating liquefaction and controlling deformation in embankment foundations under seismic conditions.

Keywords: Hybrid Piles (HPs); Shaking Table; Excess Pore Water Pressure; Settlement.

1. Introduction

Liquefaction of saturated sandy soils is one of the most critical geotechnical hazards triggered by earthquakes, often leading to severe damage to embankments, foundations, port facilities, and other earth-supported infrastructure [1]. During seismic shaking, excess pore water pressure accumulates rapidly in loose, saturated sands, causing a significant reduction in effective stress and shear strength, which may ultimately result in large deformations or flow failure [2]. Historical earthquake events and post-earthquake field observations have repeatedly demonstrated that embankments founded on liquefiable soils are particularly vulnerable due to their relatively low confinement and sensitivity to cyclic loading.

To better understand liquefaction mechanisms, numerous laboratory-based investigations have been conducted, including cyclic triaxial tests [3], cyclic direct simple shear tests [4], and resonant column tests [5]. Although these element-level tests provide valuable insight into soil behavior under cyclic loading, their inherent limitations in reproducing realistic stress paths, drainage conditions, and boundary effects restrict their ability to represent field-scale

* Corresponding author: yunusm22d@student.unhas.ac.id

https://doi.org/10.28991/CEJ-2026-012-05-024

seismic responses. In contrast, 1-g shaking table tests allow for direct observation of soil-structure interaction, excess pore water pressure generation, and deformation patterns under controlled dynamic loading, making them a widely adopted experimental approach for evaluating liquefaction and mitigation performance.

Various ground improvement methods have been investigated to mitigate liquefaction, including geosynthetics [6], prefabricated vertical drains (PVD) [7], and rubber drains [8-10]. Pile-based reinforcement systems such as micropiles [11, 12], stone columns [13-15], and sand compaction piles [16, 17] have been widely studied for improving soil stiffness and deformation resistance. In addition, precast cement piles [18], sheet piles [19], and timber piles [20] have been applied as alternative countermeasures in liquefiable soils. Previous shaking table studies have shown that vertical drainage systems are effective in accelerating excess pore water pressure dissipation, whereas pile-type reinforcements primarily improve stiffness and deformation resistance. However, many of these methods rely on a single dominant mechanism and often involve high construction costs, complex installation procedures, or environmentally intensive materials.

Recent experimental studies increasingly emphasize that liquefaction mitigation performance under repeated shaking events depends on the coupled contribution of drainage, densification, and reinforcement mechanisms. For instance, PVD has been shown to improve liquefaction and reliquefaction resistance under multiple shaking sequences by accelerating pore pressure dissipation, although performance may vary with excitation patterns and loading history [21]. Complementary findings also indicate that combining drainage with densification mechanisms can further enhance resistance against repeated liquefaction, highlighting the importance of mechanism integration rather than relying on a single improvement pathway [22]. In parallel, recent 1-g shaking table evidence on pile-type countermeasures confirms that seismic effectiveness is sensitive to input motion characteristics and configuration, suggesting that stiffness-based reinforcement alone may not be sufficient without adequate pore pressure control [23]. Moreover, emerging sustainable solutions such as pervious concrete piles demonstrate that synergistic densification–drainage–shear reinforcement can substantially suppress excess pore water pressure ratio and settlement under shaking, strengthening the rationale for integrated systems that merge mechanical support and drainage within a single element [24]. These recent advances reinforce the need for an integrated hybrid concept—such as the proposed HPs system—to simultaneously improve stiffness and accelerate drainage under repeated seismic loading.

To address these gaps, this study proposes and evaluates an innovative hybrid pile system (HPs) that integrates timber piles as structural elements with PVD to enhance drainage performance. The central hypothesis is that the combined mechanical and hydraulic functions of HPs can more effectively suppress excess pore water pressure buildup, promote progressive densification, and reduce seismic-induced settlement compared to unreinforced soil conditions. A series of shaking table tests was conducted on embankment models constructed over saturated sand with an initial relative density of 40%, subjected to peak ground accelerations ranging from 0.3 g to 0.5 g. The performance of the proposed system was assessed through measurements of penetration resistance, acceleration response, excess pore water pressure ratio, changes in relative density and void ratio, and settlement behavior.

By providing systematic experimental evidence on the coupled effects of stiffness enhancement and drainage improvement, this study contributes to a clearer understanding of the mechanisms governing liquefaction mitigation using hybrid reinforcement systems. The findings are expected to support the development of more effective, sustainable, and practical ground improvement strategies for embankments located in seismically active regions.

2. Materials and Methods

2.1. Sand

This study utilized locally sourced sand obtained from the coastal area of Galesong, Takalar Regency, South Sulawesi Province, Indonesia. Representative samples of the Galesong sand used in this study are shown in Figure 1, illustrating the physical appearance and uniformity of the material. The grain size distribution of the Galesong sand is also presented in Figure 2. The characterization of the Galesong sand was conducted in accordance with the American Society for Testing and Materials (ASTM), and the test results are summarized in Table 1.

Figure 1. Representative samples of Galesong sand

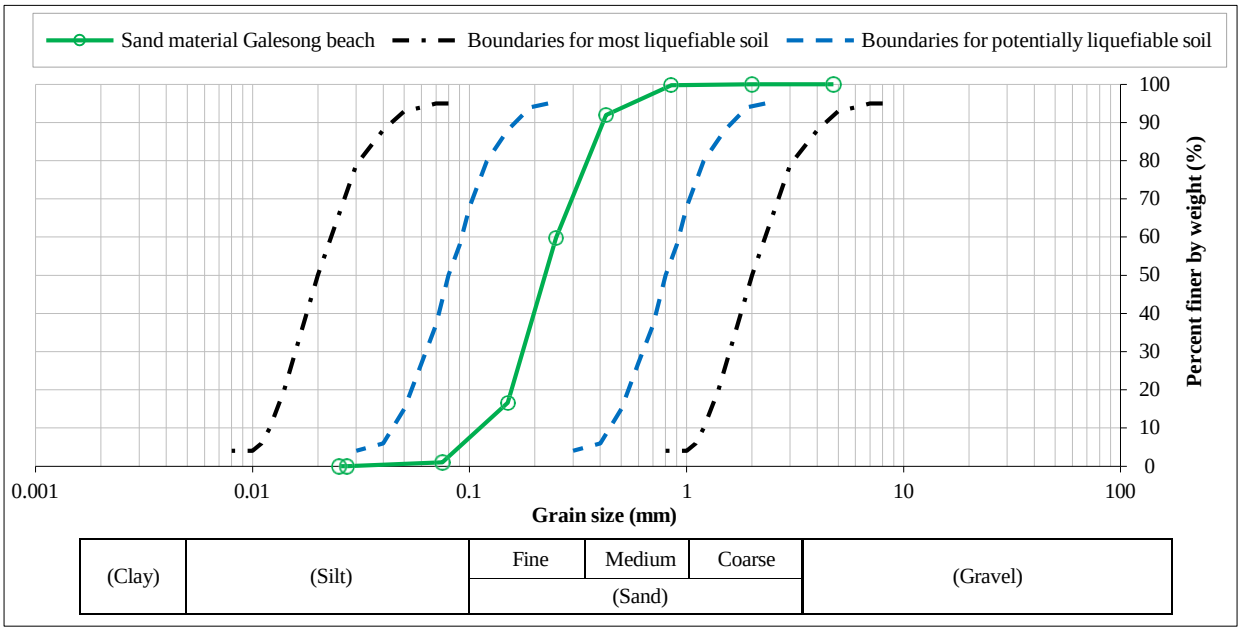

Figure 2. Grain size distribution of Galesong sand

Table 1. Index properties of Galesong sand

Description	Unit	Value	ASTM
Water content (w)	%	18.26	D2216 - 19
Specific gravity (Gs)	-	3.17	D854 - 23
Grain size distribution			
D_{10}	mm	0.120	D6913M - 17
D_{30}	mm	0.180	
D_{50}	mm	0.265	
Coefficient of uniformity (C_u)	-	2.21	
Coefficient of curvature (C_c)	-	1.02	
Unit weight (γ_d)			
($\gamma_{dmin.}$)	kN/m^3	18.25	D2453 – 16 [25]
($\gamma_{dmax.}$)	kN/m^3	20.21	
Void ratio (e)			
$e_{min.}$	-	0.65	D4254 – 16 [26]
$e_{max.}$	-	0.86	

Galesong sand can be classified as black iron sand containing a high proportion of heavy minerals, predominantly magnetite, resulting in a specific gravity exceeding 2.70. This type of sand is usually found around beaches or alluvial deposits with high heavy mineral content. The particle size distribution of Galesong sand shows that it belongs to the uniformly graded category, with a uniformity coefficient (C_u = 2.21 < 4) and a curvature coefficient (C_c = 1.02).

2.2. Hybrid Piles (HPs)

In this study, the hybrid piles (HPs) were constructed using a combination of two materials: prefabricated vertical drain (PVD) sheets and *Eucalyptus pellita* timber. Three timber shafts made of *Eucalyptus pellita*, each with a diameter of 1 cm and a length of 40 cm, were arranged in a bundle. PVD sheets were inserted between the timber shafts and secured using steel wire ties at the top, middle, and bottom positions. The timber components of the HPs were intended to provide structural stiffness, while the PVD sheets served as vertical drainage channels to facilitate rapid dissipation of excess pore water pressure during dynamic loading. The configuration of the hybrid piles system adopted in this study is shown in Figure 3.

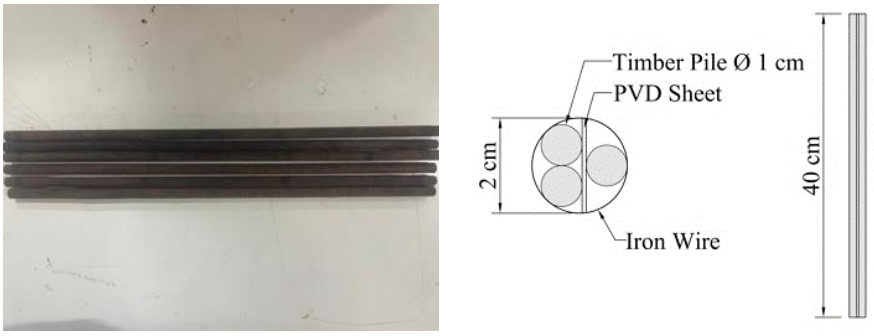

(a) (b)

Figure 3. Materials used for hybrid piles *(a) Eucalyptus pellita* timber, (b) Hybrid piles assembly details

2.3. Shaking Table and Instrumentation

Experimental testing was conducted using a shaking table located in the Geotechnical and Geoenvironmental Laboratory of the Department of Civil Engineering at Hasanuddin University's Faculty of Engineering. The shaking table measures 1.2 m x 1.2 m and has a capacity of 3 tonnes. Horizontal movement is generated by a servo-hydraulic actuator mounted on the table. It has a maximum peak speed of 1 m/s and a maximum displacement of 40 mm, an operating frequency of 0.01–50 Hz, and an acceleration range of 0.001–1 g. The acceleration, frequency, and dynamic load can be selected according to the test conditions using digitally controlled data acquisition, as illustrated in Figure 4.

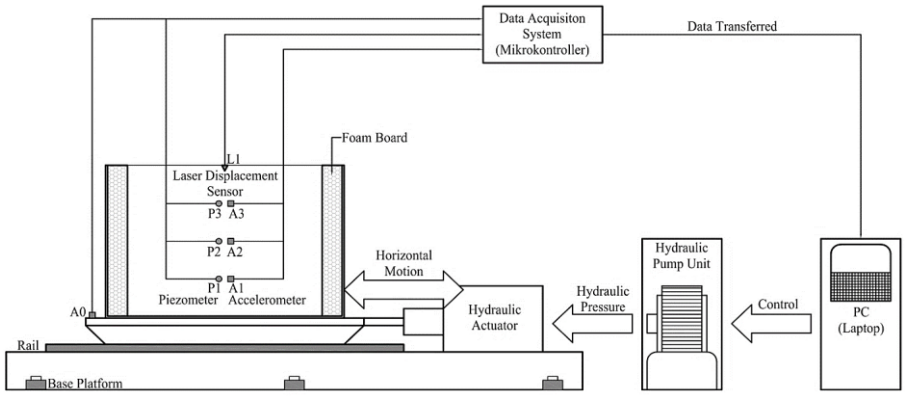

Figure 4. Schematic diagram of experimental setup

In this study, three types of measurement instruments in the form of sensors were installed, namely piezometers, accelerometers, and laser displacement sensors. Piezometers were used to monitor the development of pore water pressure during dynamic loading. Three piezometers, namely P1, P2, and P3, were installed vertically at depths of 50 cm, 30 cm, and 10 cm from the ground surface using guide rods to ensure that the sensors did not shift during backfilling. Three accelerometers, namely A1, A2, and A3, were placed adjacent to the piezometers at the same depth to record the depth-dependent acceleration response of the soil. The laser displacement sensor (L1) was positioned above the top of the embankment on the central axis of the model to measure continuous vertical deformation during the dynamic loading process, as shown in Figure 5-a.

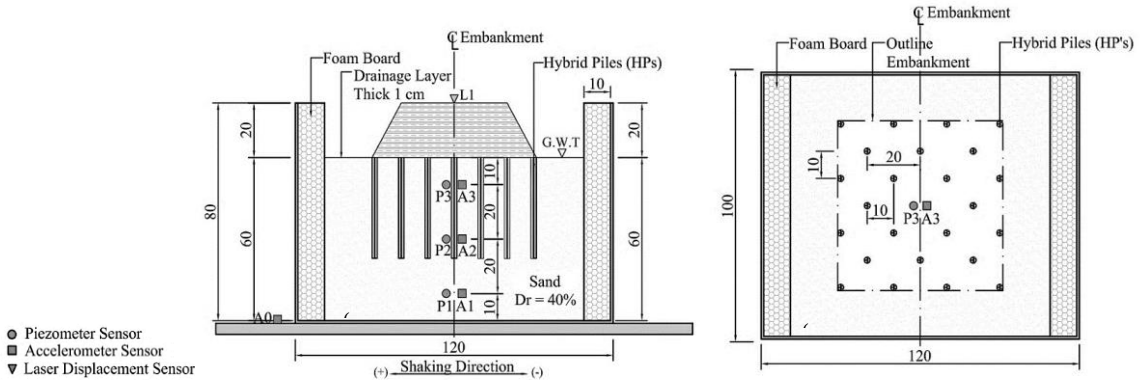

Figure 5. Layout of the experimental model, (a) Cross-sectional view of the model, (b) Top view of the mode

Table 2 summarizes the specifications and measurement accuracy of the accelerometers, piezometers, and laser displacement sensors used in this study. These specifications demonstrate that the selected sensors offer the necessary resolution and accuracy to reliably capture acceleration responses, excess pore water pressure development, and settlement during shaking table tests.

Table 2. Sensor-related parameters

Sensor type	Parameter	Specification
Accelerometer	Accuracy	0.01g
	Resolution	16-bit
	Stability	0.005g
Piezometer	Precision	≤0.3% FS
	Range	0.01 – 10 MPa
Laser Displacement Sensor	Measuring range	±35 mm; 1.328 in
	Repeatability	70 µm; 2.756 mil
	Linearity	±0.1% FS

2.4. Experimental Setup

A transparent test tank with dimensions of 120 × 100 × 80 cm (length × width × height) was specially fabricated for the experimental testing. The tank was constructed using 10 mm-thick acrylic glass panels, which were securely fastened to a rigid steel frame using steel brackets, as shown in Figure 6. To minimize the influence of boundary effects arising from the rigidity of the container on soil behavior, foam boards made of polyurethane were installed along the sidewalls of the tank. These foam inserts reduce the influence of wave reflections from the tank's rigid boundaries, as recommended by prior studies [27, 28].

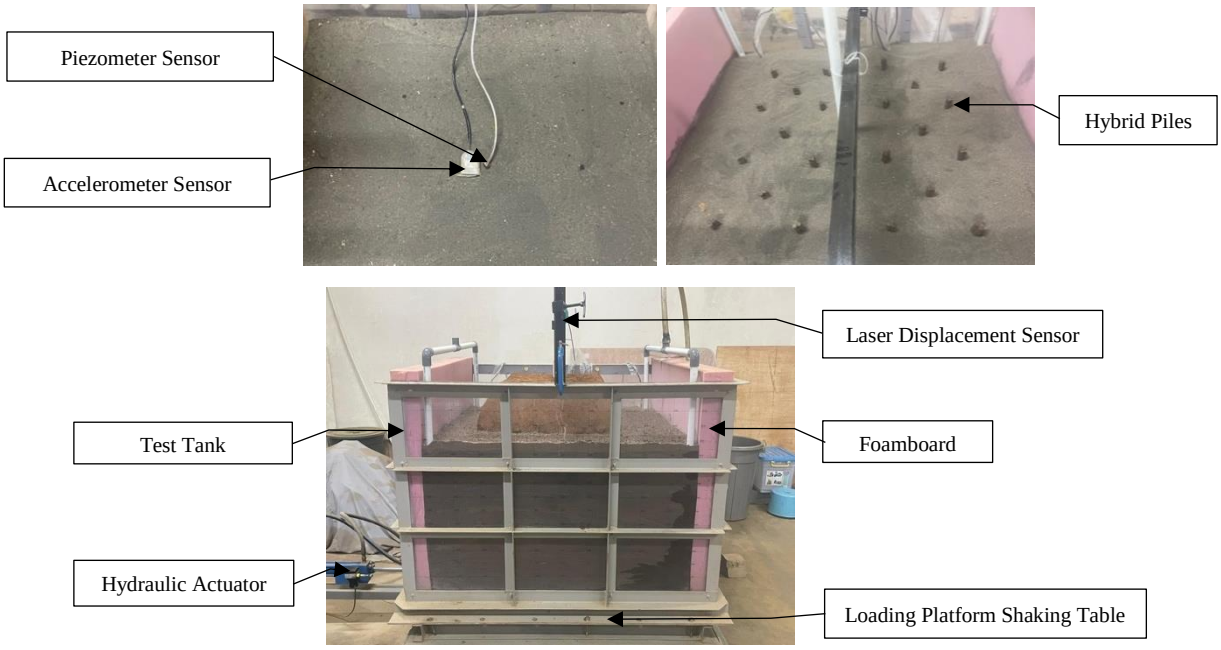

Figure 6. Experimental setup

Two laboratory-scale physical models were prepared: an unreinforced soil model and a model reinforced with HPs, as illustrated in Figure 6. Both models were constructed using the sand bed saturation method. The soil material consisted of uniform sand, which was initially conditioned in a dry state and sieved to ensure a homogeneous particle size distribution. Sand placement was conducted in stages using the layered deposition technique, with each layer having a thickness of approximately 100 mm. The required mass of dry sand for each layer was determined using the weighting method, based on the test tank volume and a target relative density of 40%. The pre-weighed sand was then carefully poured into the tank while maintaining a controlled and minimal drop height to achieve the desired relative density. In this study, a fall height of 200 mm was adopted, consistent with procedures reported in comparable experimental studies.

A relative density of approximately 40% was adopted for the liquefaction tests because it corresponds to loose-to-medium sand conditions, which are highly prone to excess pore water pressure generation and effective stress reduction

under seismic loading. At this density, the soil exhibits predominantly contractive behavior, leading to rapid accumulation of excess pore water pressure (Δu) and promoting the onset of liquefaction. These conditions provide a clear and reliable basis for evaluating soil response mechanisms. The selected relative density ($D_r \approx 40\%$) is in line with commonly accepted recommendations in the literature [29, 30], and has been widely used in previous liquefaction studies**.** Consequently, the experimental results are considered consistent, representative, and directly comparable with those reported in earlier research [2, 16, 20].

Once the sand deposition was complete, the HPs were installed in the prepared soil bed. They were arranged in a triangular configuration to balance effectiveness and spatial efficiency within the test tank (see Figure 5-b). The dimensions and triangular layout of the HPs were determined based on model-scale limitations, constructability, and the soil–pile interaction mechanisms reported in previous experimental studies rather than through a formal optimization process. The pile diameter and spacing were selected to promote effective interaction between adjacent piles while preventing excessive confinement effects in the small-scale physical model [31]. A triangular arrangement was adopted to provide a more uniform distribution of stiffness and drainage pathways, as well as facilitating symmetric boundary conditions and consistent installation in the 1-g shaking table tests [32]. Although no parametric optimization of pile spacing was performed, the selected configuration is deemed suitable for the comparative evaluation of the HPs system under identical loading conditions.

2.5. Experimental Workflow

This subsection presents the experimental workflow adopted in this study to ensure a systematic and reproducible investigation. The workflow, summarized in Figure 7, outlines the sequential stages of the research, beginning with material characterization and physical model preparation, followed by the configuration of unreinforced and HPs-reinforced models, shaking table testing under different peak ground acceleration levels, and data acquisition. The workflow further highlights the comparative framework used to evaluate soil response and mitigation performance by subjecting all test conditions to identical preparation procedures, boundary conditions, and loading protocols. This structured approach facilitates consistent interpretation of the measured responses, including pore water pressure, acceleration, and settlement.

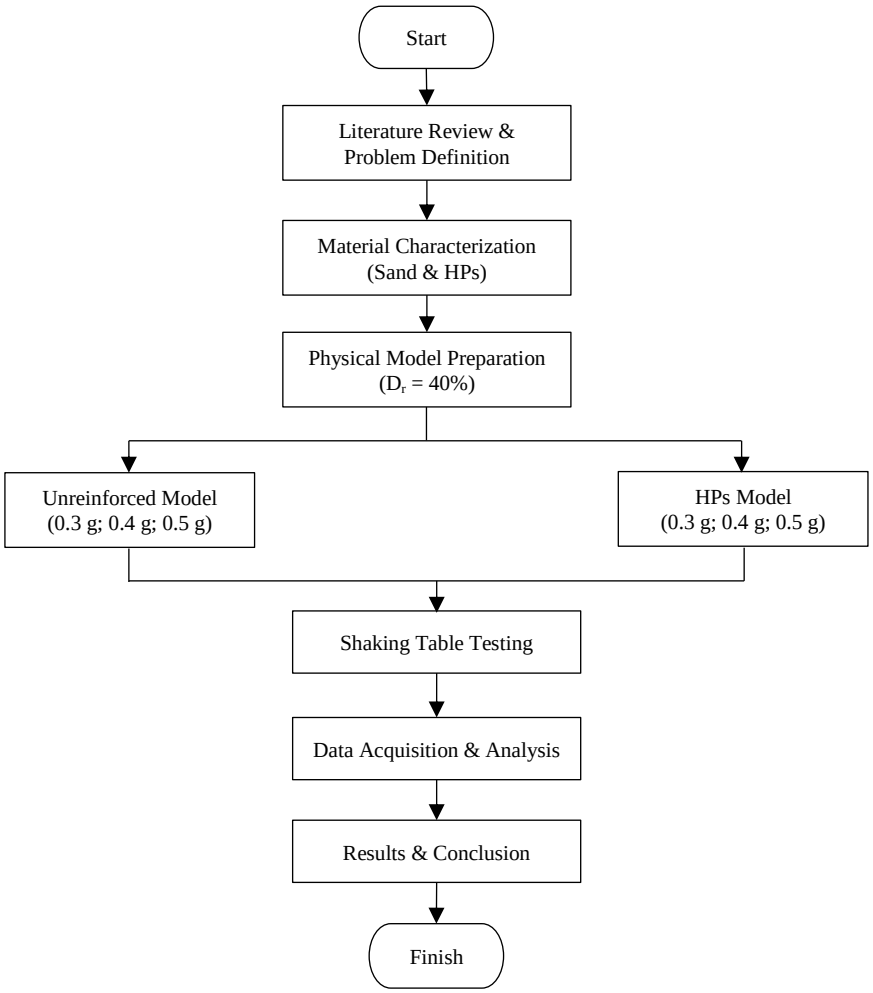

Figure 7. Research flow diagram

2.6. Evaluation of Density

A Hand Cone Penetrometer (HCP) test was used to estimate the relative density of the prepared soil layers. The device consists of a 60° cone with a surface area of 1.5 cm² attached to an extension rod. Penetration resistance at various depths was measured using a proving ring and a dial gauge, as shown in Figure 8. The penetrometer was pushed continuously into the soil at a penetration rate of 10 to 20 mm/s. following the procedures outlined in ASTM D3441-05 [33]. The tests were conducted at four locations on each side of the embankment model. The average cone penetration resistance (q_c) was used to estimate the relative density of the soil at each depth. Evaluations were conducted at 100 mm intervals, and the corresponding relative density was calculated using Equation 1, as proposed by Jamiolkowski et al. [34].

$$Dr = 100 \times \left[0.268 \times ln \left(\frac{q_c/\sigma_{atm}}{\sqrt{\sigma'_{vo}/\sigma_{atm}}} \right) - 0.675 \right] \quad (1)$$

where, D_r is relative density of the soil sample (%), σ'_{vo} is effective vertical overburden stress (kPa), q_c is cone penetration resistance (kPa), and σ_{atm} is atmospheric pressure (atm).

Figure 8. Hand Cone Penetrometer (HCP) Testing

2.7. Model Testing Procedure

Dynamic loading tests were conducted using a shaking table to apply controlled sinusoidal wave excitation to the soil model. After calibrating and synchronizing all sensors, the shaking table was operated, starting with low-intensity vibrations and increasing to the peak ground acceleration (PGA) values specified for each test stage, as shown in Table 3. During a period of constant vibration, the input acceleration history was applied, while the data acquisition system recorded the soil response in real time. This included monitoring increases in pore water pressure, internal soil acceleration, and settlement.

Table 3. Experimental matrix of the model tests

Code	D_r (%)	Acceleration (g)	Time (second)
0.3g UR	40	0.3	60
0.4G UR	40	0.4	60
0.5G UR	40	0.5	60
0.3g HPs	40	0.3	60
0.4g HPs	40	0.4	60
0.5g HPs	40	0.5	60

3. Results

3.1. Effect of Soil Condition on Liquefaction Resistance

The results obtained from the HCP tests provided the cone penetration resistance (q_c) and the evaluated relative density of the soil for both the unreinforced model (UR) and the model reinforced with (HPs) at their initial conditions, as illustrated in Figure 9.

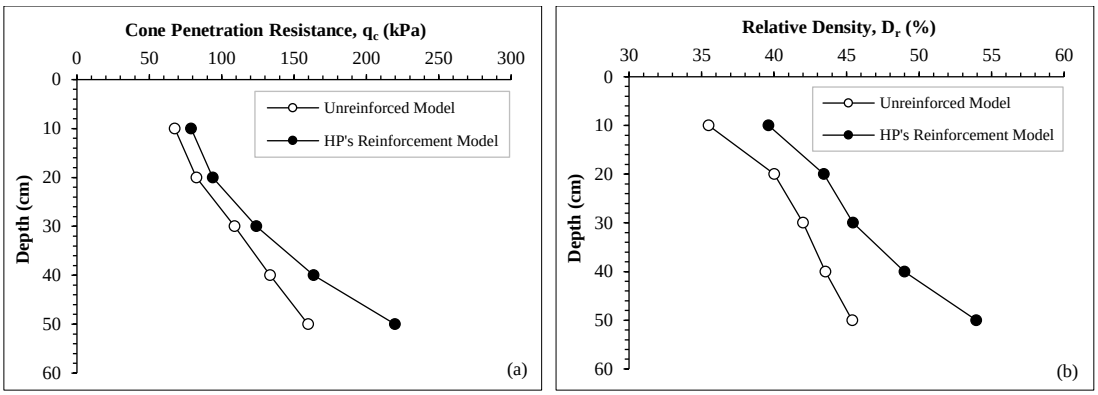

Figure 9. Distribution of cone penetration resistance (q_c) and relative density (D_r) with depth for unreinforced and HPs-reinforced models, (a) cone penetration resistance (q_c), (b) relative density (D_r)

Figure 9-a shows that the q_c of the HPs-reinforced model is consistently higher than that of the unreinforced model, with the difference increasing with depth. This trend is consistent with the relative density distribution shown in Figure 9(b), where higher D_r values are observed in the HPs model, particularly in the lower layers. The concurrent increase in q_c and D_r indicates that the HPs promote both local densification and stress redistribution through enhanced confinement and soil–structure interaction mechanisms. Consequently, soil stiffness is enhanced, improving resistance to cyclic degradation and liquefaction initiation. In contrast, the unreinforced soil exhibits only limited stiffness improvement governed primarily by self-weight consolidation.

In addition to global densification and soil–structure interaction effects, localized stress concentration around the HPs may also contribute to the observed increase in q_c. The presence of relatively stiff pile elements modifies the local stress field and increases the effective stress in the surrounding soil, particularly within the pile influence zone. This stress redistribution can locally increase q_c values measured by the cone, even without uniform changes in void ratio. Similar observations have been reported in reinforced and confined soils, where higher q_c values were attributed partly to stress concentration effects induced by nearby structural elements rather than densification alone [35]. In the present study, cone penetration tests were conducted at locations offset from the pile surfaces to minimize direct interference; however, the influence of localized stress redistribution cannot be completely eliminated. Therefore, the measured qc enhancement is interpreted as the combined effect of densification, confinement, and stress concentration induced by the HPs.

3.2. Changes in Relative Density Due to Variation in Peak Ground Acceleration

The cone penetration resistance (q_c) values obtained from the variations in peak ground acceleration applied to the unreinforced model (UR) and reinforcement hybrid pile models (HPs) are presented in Figure 10(a), while the corresponding changes in relative density for both models are shown in Figure 10(b).

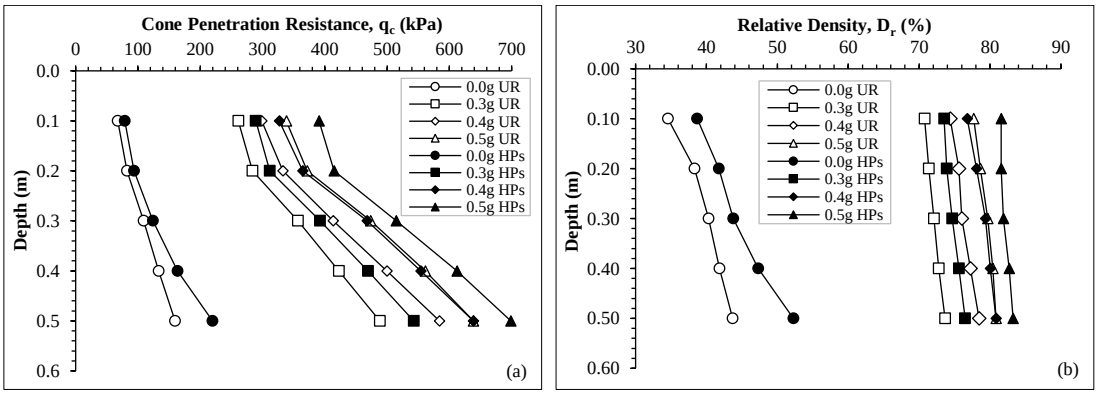

Figure 10. Effect of peak ground acceleration on, (a) cone penetration resistance (q_c), (b) relative density (D_r)

As illustrated in Figures 10-a and 10-b, an increase in PGA results in only a marginal rise in cone resistance (qc) and relative density (D_r) in the unreinforced model, as the generation of excess pore water pressure restricts further soil densification. In contrast, the HPs-reinforced model demonstrates a pronounced increase in both q_c and D_r with increasing PGA, particularly at greater depths. This behavior indicates that confinement provided by the HPs enables cyclic shear strains to induce progressive densification. Consequently, the reinforced soil mass becomes denser and more stable, reducing its susceptibility to liquefaction and re-liquefaction.

3.3. Variation in Void Ratio of Soil

The void ratio is a key parameter in evaluating both the potential for soil liquefaction and the effectiveness of the reinforcement method employed. The variation in void ratio across different soil depths was estimated using Equation 2:

$$e = e_{max} - D_r\,(e_{max} - e_{min}) \tag{2}$$

where e is the void ratio value, D_r is the relative density of the soil at each depth, and e_{min} and e_{max} are the minimum and maximum void ratio values presented in Table 1. The variation in void ratio at each soil layer depth due to the application of PGA is illustrated in Figure 11.

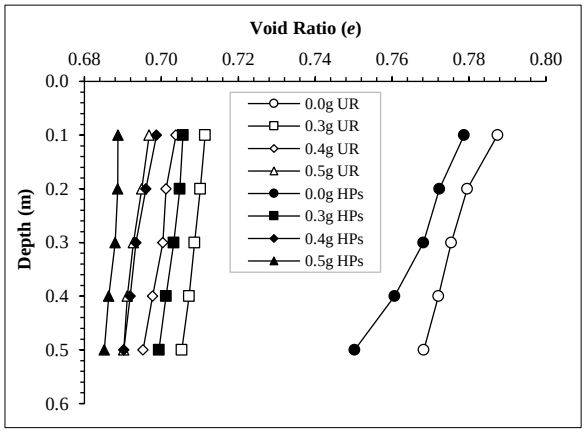

Figure 11. Variation of void ratio with depth under different peak ground acceleration levels

Figure 11 illustrates that the void ratio decreases with depth for both models; however, the reduction is more uniform in the HPs-reinforced soil. This behavior indicates that volumetric compression in the reinforced model is governed by controlled densification under confinement rather than abrupt contractive collapse mechanisms. The combined action of structural restraint and drainage provided by the HPs limits excessive pore pressure buildup, resulting in a more stable void ratio evolution. In contrast, the unreinforced soil shows a less consistent void ratio reduction, indicating a higher tendency toward contractive behavior during cyclic loading.

3.4. Acceleration Time History

Figures 12 to 14 show the acceleration time histories recorded by the accelerometer sensors installed in the soil layers of the unreinforced and HPs reinforced models under variations in PGA of 0.3 g, 0.4 g, and 0.5 g, as tested in this study. The sensor locations were as follows: Accelerometer 1 at a depth of 50 cm, Accelerometer 2 at a depth of 30 cm, and Accelerometer 3 at a depth of 10 cm.

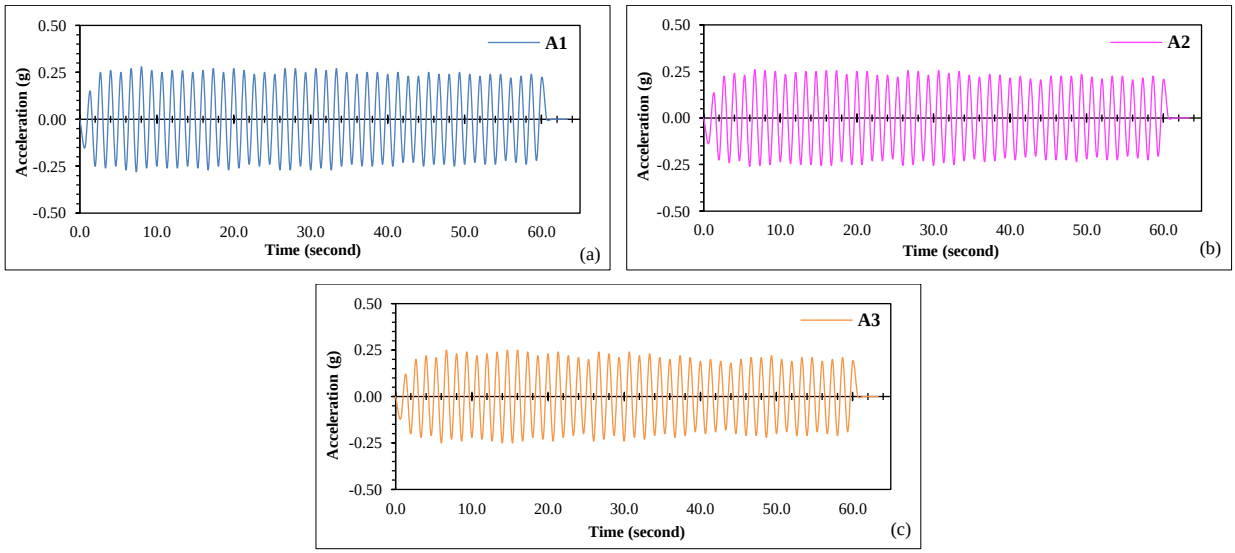

Figure 12. Acceleration time histories recorded at different depths under PGA levels of 0.3 g, (a) A1 *D* = 50 cm, (b) A2 *D* = 30 cm, (c) A3 *D* = 10 cm

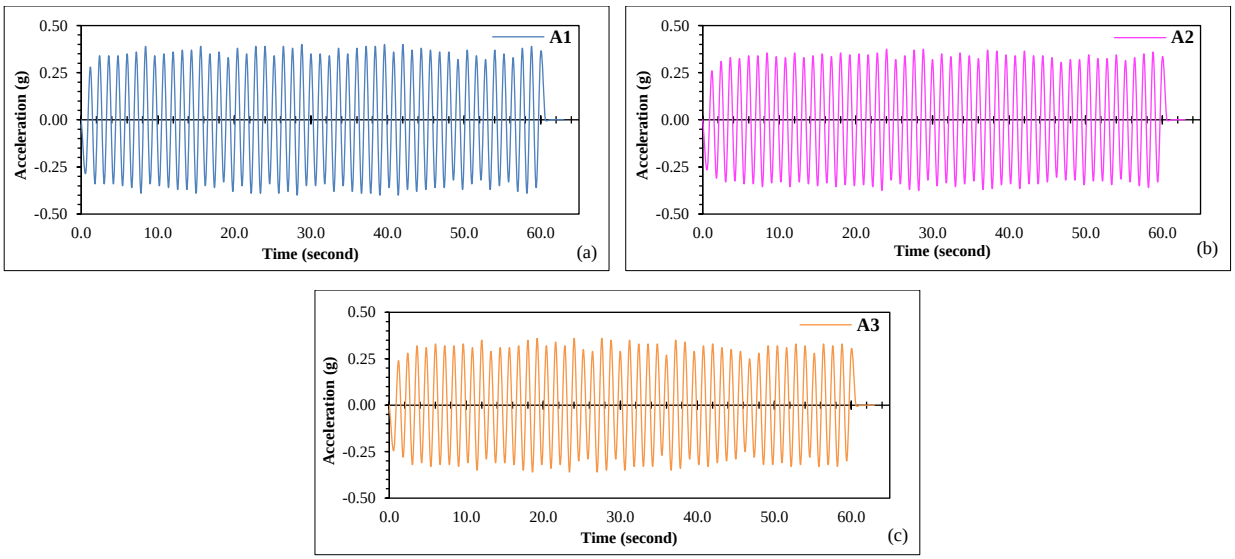

Figure 13. Acceleration time histories recorded at different depths under PGA levels of 0.4 g, (a) A1 *D* = 50 cm, (b) A2 *D* = 30 cm, (c) A3 *D* = 10 cm

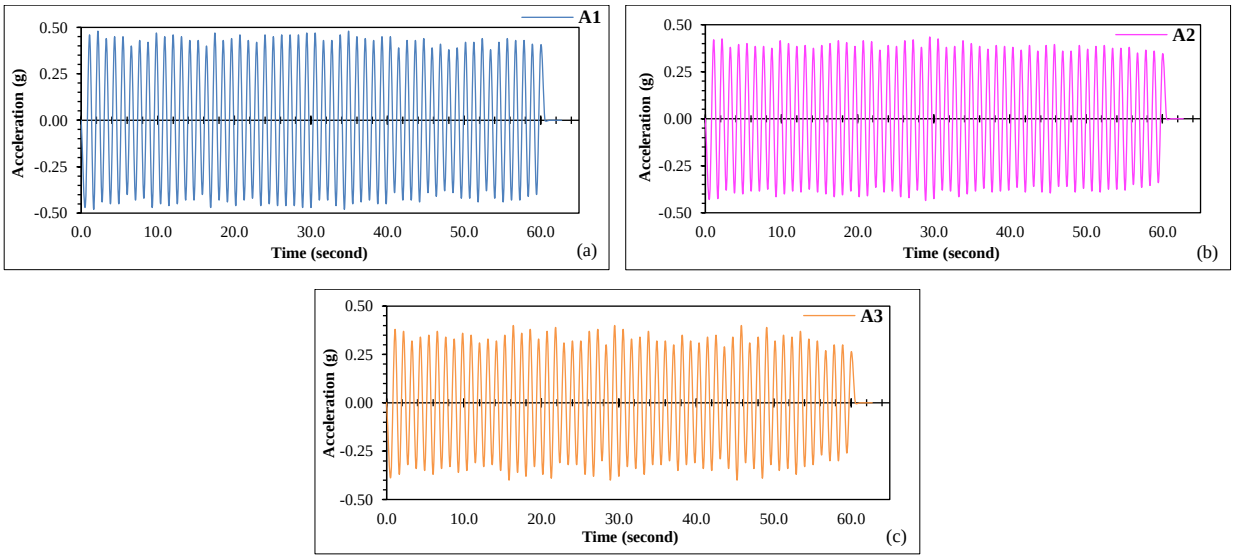

Figure 14. Acceleration time histories recorded at different depths under PGA levels of 0.5 g, (a) A1 *D* = 50 cm, (b) A2 *D* = 30 cm, (c) A3 *D* = 10 cm

The acceleration time histories presented in Figures 12–14 indicate that acceleration amplitudes decrease with depth in both models, with a more pronounced attenuation observed in the HPs-reinforced model. This behavior reflects increased soil stiffness and enhanced energy dissipation due to soil–pile interaction. The HPs dissipate seismic energy through frictional and plastic deformation mechanisms, thereby reducing acceleration amplification toward the ground surface. Such attenuation is beneficial for embankment stability, as it lowers the deformation demand during strong ground motion.

3.5. Time History of Pore Water Pressure Ratio

This section discusses the development and dissipation of excess pore water pressure during the application of PGA. The recorded values of excess pore water pressure from the piezometer sensors were analyzed to determine the pore water pressure ratio (*ru*) over time for each variation of PGA. The *ru* was estimated using the following Equation:

$$ru = \frac{\Delta u}{\sigma'_{V0}} \tag{3}$$

where, *ru* is the pore water pressure ratio, Δu is the excess pore water pressure value obtained from piezometer sensor readings (kPa), and σ'_{V0} is the soil overburden pressure (kPa). Figures 15 to 16 show the time history of the pore water pressure ratio (*ru*) for each variation in the rate of PGA on the UR model and the model HPs reinforced.

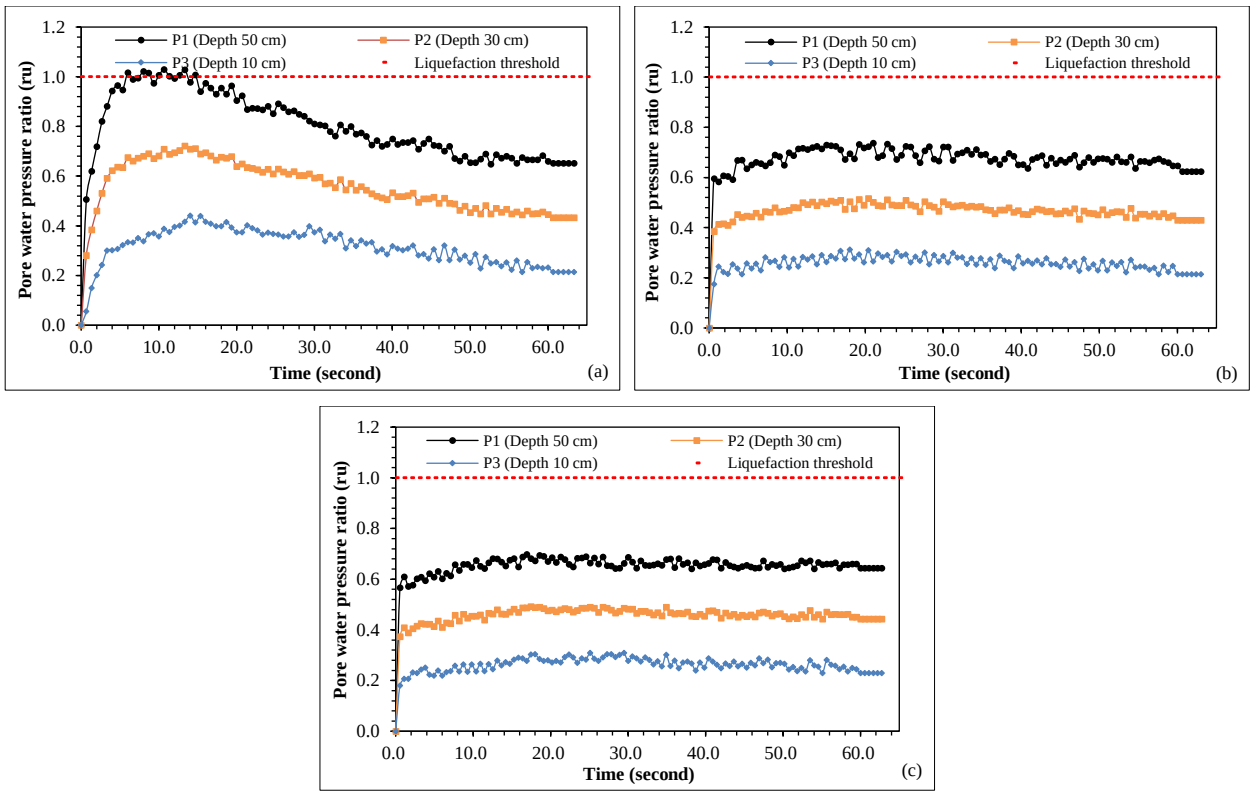

Figure 15. Time histories of pore water pressure ratio for unreinforced models, (a) 0.3 g, (b) 0.4 g, (c) 0.5 g

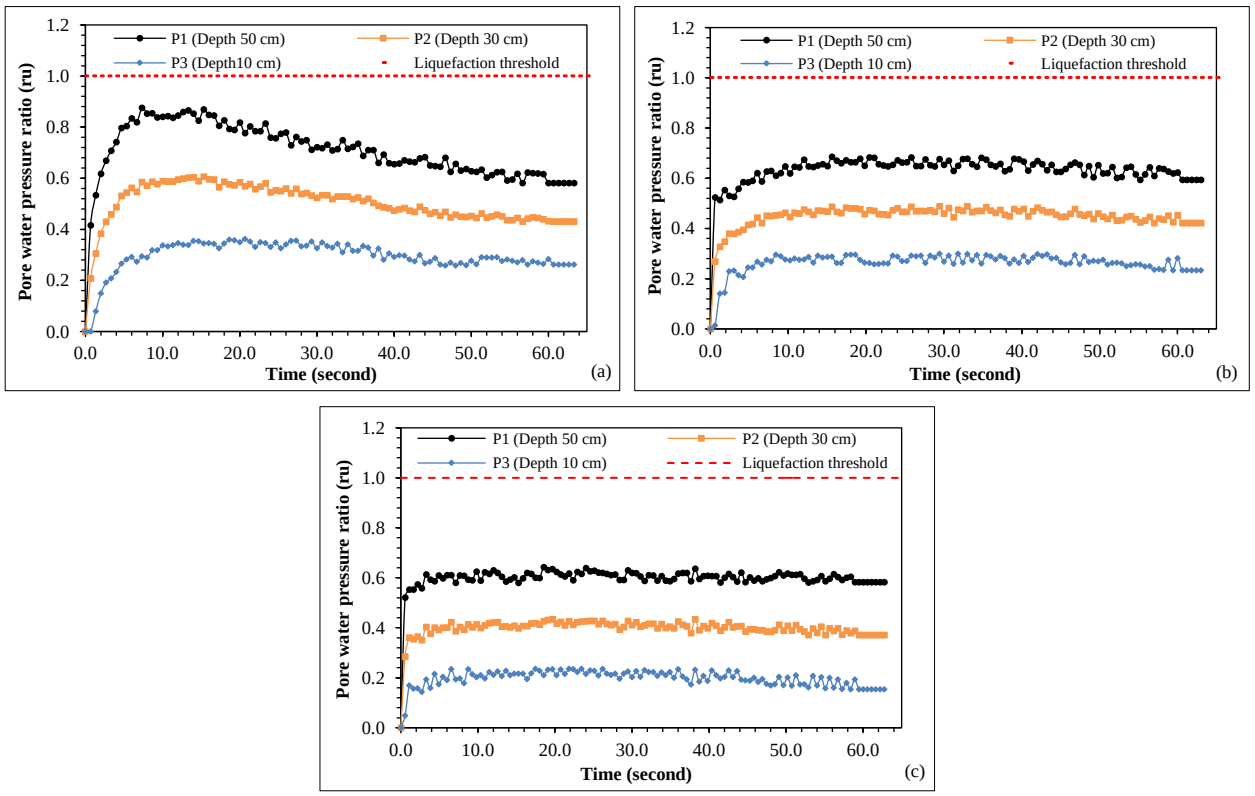

Figure 16. Time histories of pore water pressure ratio for HPs-reinforced models., (a) 0.3 g, (b) 0.4 g, (c) 0.5 g

Figure 15 shows that the unreinforced model rapidly attains the pore water pressure ratio (*ru*) approaching unity, indicating the initiation of liquefaction. In contrast, Figure 16 demonstrates that the model reinforced with HPs exhibits substantially lower *ru* values at the same peak ground acceleration (PGA) levels. This reduction in *ru* is attributed to improved drainage provided by the prefabricated vertical drains (PVD) and increased confinement induced by the timber piles. The stabilized *ru* response observed under higher PGA levels suggests that the HPs system effectively delays liquefaction onset and inhibits pore pressure regeneration during repeated seismic loading.

3.6. Settlement Time History

Figure 17 shows the time-dependent settlement response recorded by the laser displacement sensor (L1), which illustrates how vertical deformation evolves during dynamic loading. Additionally, Figure 18 summarizes the maximum settlement reductions for the unreinforced and HP-reinforced models under varying peak ground accelerations, offering a clear comparative assessment of the effectiveness of reinforcement.

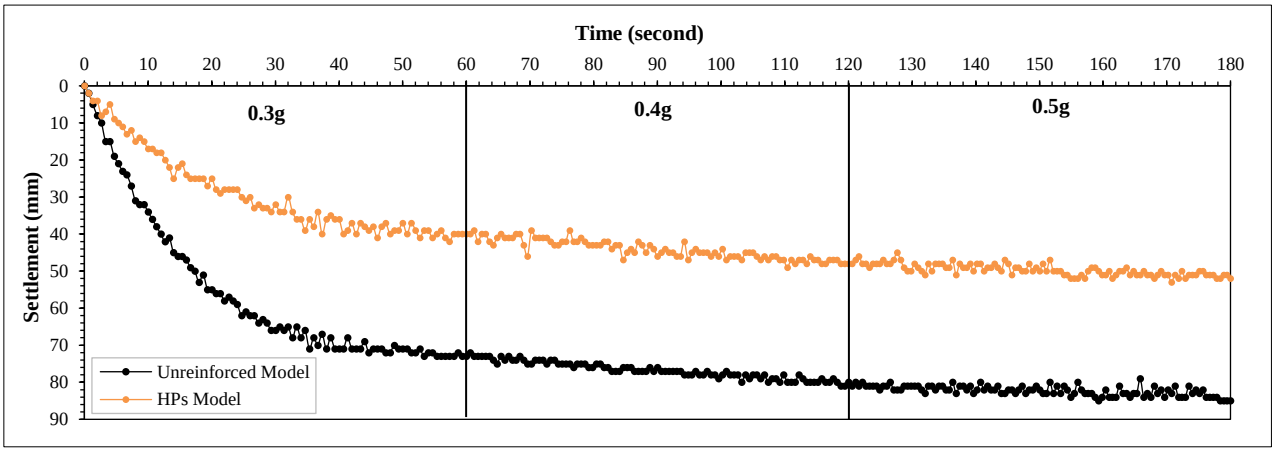

Figure 17. Time history of settlement under different peak ground acceleration levels

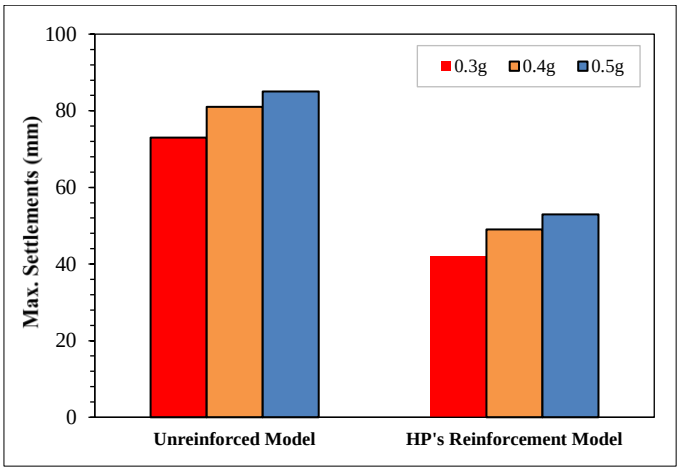

Figure 18. Maximum values of settlement under different peak ground acceleration levels

Figure 17 shows that settlement development during shaking is significantly reduced in the HPs-reinforced model compared to the unreinforced model. This trend is quantitatively confirmed by the maximum settlement values summarized in Figure 18, where reductions of approximately 37–42% are observed across all PGA levels. The reduced settlement results from the combined effects of increased stiffness, controlled densification, and accelerated pore pressure dissipation. These results confirm that the HPs systems provide effective deformation control in liquefiable soils subjected to seismic loading.

4. Discussion

The results obtained in this study are generally consistent with previous shaking table investigations on liquefaction mitigation, while demonstrating additional advantages associated with the proposed HPs system. Previous studies on vertical drainage countermeasures, such as prefabricated vertical drains and gravel drains, reported effective reduction of excess pore water pressure primarily through accelerated dissipation mechanisms, with limited influence on soil stiffness [21, 36]. Similar observations were also reported for rubber drain systems, where pore pressure control was achieved without significant improvement in penetration resistance or density [8-10].

In contrast, pile-based reinforcement methods, including micropiles and stone columns, have been shown to significantly enhance soil stiffness and reduce deformation through confinement and load transfer mechanisms [11, 12, 23]. However, several studies indicated that these systems alone may not sufficiently suppress excess pore water pressure generation under strong cyclic loading [13-15]. These findings suggest that stiffness enhancement and pore pressure control have often been addressed independently in conventional liquefaction mitigation approaches.

The observed behavior reflects the combined effects of drainage enhancement and stiffness improvement. The reduction in pore water pressure ratio (ru) of up to 16.26% obtained in the HPs-reinforced model is comparable to reductions reported for drainage-based systems in previous shaking table tests [8, 9]. At the same time, the observed increases in cone penetration resistance and relative density are consistent with trends reported for pile-reinforced soils, where confinement-induced densification led to improved cyclic resistance [11, 12].

Regarding deformation response, the settlement reduction of approximately 37–42% achieved in this study is within the range reported for pile-type countermeasures under similar loading conditions [18, 19]. Earlier studies attributed settlement reduction mainly to stiffness enhancement and improved load-bearing capacity [18]. The present results indicate that settlement control is further enhanced when stiffness improvement is combined with effective pore water pressure dissipation, which helps preserve effective stress during shaking [19].

Furthermore, the relatively stable (ru) response under increasing PGA observed in the HPs-reinforced model indicates improved resistance to pore pressure regeneration and re-liquefaction. Similar trends were reported in recent studies emphasizing the role of progressive densification and continuous drainage under repeated seismic loading [7, 17]. The present study extends these findings by demonstrating that such behavior can be achieved using a single integrated reinforcement element combining structural support and drainage functions.

Overall, while previous studies have demonstrated the individual effectiveness of drainage-based or stiffness-based mitigation techniques, the present results provide experimental evidence that integrating both mechanisms within a HPs system leads to a more comprehensive improvement in liquefaction resistance and deformation control [11, 18]. This integrated response represents a clear advancement over conventional single-mechanism approaches commonly reported in the literature.

The initial relative density adopted in this study ($D_r \approx 40\%$) represents loose sand conditions that are highly susceptible to liquefaction and is therefore appropriate for evaluating the effectiveness of liquefaction mitigation measures. Under denser sand conditions, the soil response is expected to differ in terms of liquefaction susceptibility and deformation behavior. Sands with higher relative density generally exhibit increased interparticle contact forces and reduced contractive tendencies under cyclic loading, resulting in lower excess pore water pressure generation and delayed liquefaction onset even without ground improvement.

Nevertheless, the fundamental mechanisms activated by the HPs system—namely stiffness enhancement, confinement, and accelerated drainage—remain applicable for denser sands. In such conditions, the relative contribution of drainage to pore pressure control may become less dominant, while stiffness enhancement and deformation control mechanisms are expected to play a more significant role. Consequently, although the magnitude of pore water pressure reduction and densification observed in this study may be less pronounced at higher relative densities, the overall performance trends are expected to remain consistent. This discussion suggests that the applicability of the proposed HPs system extends beyond loose sand conditions and remains relevant for a broader range of soil densities, particularly in seismic design scenarios where deformation control and post-shaking stability are critical considerations.

Although 1-g shaking table tests provide valuable insight into soil–structure interaction and liquefaction mitigation mechanisms, inherent scaling limitations should be acknowledged. In 1-g physical modeling, the stress level in the soil mass is lower than that in prototype conditions, and similitude between stress, permeability, and drainage cannot be fully satisfied simultaneously. As a consequence, excess pore water pressure generation and dissipation processes may not scale perfectly, and pore pressure dissipation may occur relatively faster in the model than in the field. Similar limitations also apply to settlement behavior, as reduced overburden stress in the model may restrict volumetric compression and post-shaking reconsolidation, potentially leading to an underestimation of absolute settlement when extrapolated to prototype scale. These limitations are well documented in classical scaling laws for geotechnical physical modeling, which emphasize that 1-g shaking table tests are most suitable for investigating mechanisms and relative performance rather than direct quantitative prediction [37]. Accordingly, the present study interprets the observed reductions in pore water pressure ratio and settlement in a comparative framework, whereby reinforced and unreinforced models are subjected to identical boundary conditions and loading histories. Within this context, the relative effectiveness and underlying mechanisms of the proposed HPs system remain robust despite the acknowledged scale effects.

Although each test condition was performed once, the consistency of the measured responses can be inferred from the coherent trends observed across different PGA levels and soil conditions. Key response parameters, including excess pore water pressure ratio, acceleration attenuation, and settlement development, exhibited systematic and repeatable patterns when comparing unreinforced and HPs-reinforced models under identical loading sequences. The absence of abrupt fluctuations or contradictory trends suggests that the observed differences primarily reflect the influence of reinforcement rather than experimental randomness. Nevertheless, the lack of repeated tests limits a formal statistical assessment of variability. Future studies incorporating multiple repetitions for each test condition would be beneficial to quantify experimental scatter and further strengthen the robustness of the findings.

5. Conclusion

This study evaluated the performance of an innovative HPs systems for liquefaction mitigation and deformation control of embankment foundations subjected to seismic loading using a series of 1-g shaking table tests. The HPs system integrates structural reinforcement provided by timber piles with enhanced drainage through prefabricated vertical drains, enabling the simultaneous improvement of soil stiffness and pore water pressure dissipation. This integrated concept was assessed under repeated sinusoidal excitations with peak ground accelerations ranging from 0.3 g to 0.5 g and compared against unreinforced soil conditions.

The experimental results demonstrate that the HPs-reinforced model consistently achieved higher cone penetration resistance and relative density, indicating effective soil densification and stiffness enhancement. These improvements became more pronounced with increasing PGA, confirming that the confinement induced by the HPs promotes progressive particle rearrangement rather than contractive pore pressure buildup. Consequently, the generation of excess pore water pressure was significantly suppressed in the reinforced model, with a reduction in the maximum pore water pressure ratio of up to 16.26%. This response effectively delayed liquefaction onset and improved pore pressure dissipation behavior under repeated shaking, indicating enhanced resistance to both initial liquefaction and pore pressure regeneration.

In terms of deformation response, the HPs system reduced seismic-induced settlement by approximately 37–42% across all PGA levels. This reduction is attributed to the combined effects of increased stiffness, controlled densification, and preservation of effective stress during shaking, which collectively limited volumetric contraction and acceleration amplification. These findings confirm that settlement mitigation in liquefiable soils cannot be achieved through drainage or stiffness enhancement alone, but rather requires an integrated mechanism.

Overall, this study demonstrates that HPs provides a sustainable and effective liquefaction mitigation solution by integrating mechanical reinforcement and drainage within a single system. The results contribute to a clearer understanding of integrated mitigation mechanisms and support the application of hybrid reinforcement concepts for embankments and similar earth structures in seismically active regions.

6. Declarations

6.1. Author Contributions

Conceptualization, M.Y. and A.B.M.; methodology, M.Y. and T.H.; software, M.Y.; validation, A.B.M., T.H., and A.A.; formal analysis, M.Y.; investigation, M.Y.; resources, M.Y.; data curation, M.Y.; writing—original draft preparation, M.Y.; writing—review and editing, A.B.M., T.H., and A.A.; visualization, M.Y.; supervision, A.B.M., T.H., and A.A.; project administration, M.Y.; funding acquisition, M.Y. All authors have read and agreed to the published version of the manuscript.

6.2. Data Availability Statement

The data presented in this study are available in the article.

6.3. Funding and Acknowledgments

The authors gratefully acknowledge the support and financing of the Indonesian Education Scholarship (BPI) from the Center for Financing and Assessment of Higher Education (PPAPT) of the Ministry of Higher Education, Science and Technology, and the Education Fund Management Agency (LPDP) of the Government of the Republic of Indonesia.

6.4. Conflicts of Interest

The authors declare no conflict of interest.

7. References

[1] Ishihara, K. (1996). Soil Behaviour in Earthquake Geotechnics. Oxford University Press. Oxford, United Kingdom. doi:10.1093/oso/9780198562245.001.0001.

[2] Seed, H. B., & Idriss, I. M. (1971). Simplified Procedure for Evaluating Soil Liquefaction Potential. Journal of the Soil Mechanics and Foundations Division, 97(9), 1249–1273. doi:10.1061/jsfeaq.0001662.

[3] Zhao, J., Zhu, Z., Liu, J., & Zhong, H. (2023). Damping Ratio of Sand Containing Fine Particles in Cyclic Triaxial Liquefaction Tests. Applied Sciences (Switzerland), 13(8), 4833. doi:10.3390/app13084833.

[4] Molina-Gómez, F., Viana, A., da Fonseca Ferreira, C., & Caicedo, B. (2024). Liquefaction resistance of TP-Lisbon sand: a comparison between cyclic triaxial and cyclic direct simple shear tests. Geotechnical Engineering Challenges to Meet Current and Emerging Needs of Society, CRC Press, Boca Raton, United States. doi:10.1201/9781003431749-221.

[5] Shinde, N. S., & Kumar, J. (2022). Assessing the liquefaction potential of a sand specimen by using resonant column test. Soil Dynamics and Earthquake Engineering, 159, 107343. doi:10.1016/j.soildyn.2022.107343.

[6] Setiawan, H., Serikawa, Y., Sugita, W., Kawasaki, H., & Miyajima, M. (2018). Experimental study on mitigation of liquefaction-induced vertical ground displacement by using gravel and geosynthetics. Geoenvironmental Disasters, 5(1), 22. doi:10.1186/s40677-018-0115-3.

[7] Padmanabhan, G., & Shanmugam, G. K. (2024). Performance assessment of prefabricated vertical drains in mitigating soil reliquefaction subjected to repeated seismic events using shaking table experiments. Frontiers of Structural and Civil Engineering, 18(3), 411–427. doi:10.1007/s11709-024-1057-3.

[8] Farzalizadeh, R., Hasheminezhad, A., & Bahadori, H. (2021). Shaking table tests on wall-type gravel and rubber drains as a liquefaction countermeasure in silty sand. Geotextiles and Geomembranes, 49(6), 1483–1494. doi:10.1016/j.geotexmem.2021.06.002.

[9] Bahadori, H., Farzalizadeh, R., Barghi, A., & Hasheminezhad, A. (2018). A comparative study between gravel and rubber drainage columns for mitigation of liquefaction hazards. Journal of Rock Mechanics and Geotechnical Engineering, 10(5), 924–934. doi:10.1016/j.jrmge.2018.03.008.

[10] Hasheminezhad, A., Farzalizadeh, R., Rahimi, H., & Bahadori, H. (2022). Seismic performance assessment of wall-type gravel and rubber drains in liquefaction mitigation of sands. Bulletin of Earthquake Engineering, 20(8), 3699–3714. doi:10.1007/s10518-022-01358-3.

[11] GuhaRay, A., Mohammed, Y., Harisankar, S., & Gowre, M. S. (2017). Effect of micropiles on liquefaction of cohesionless soil using shake table tests. Innovative Infrastructure Solutions, 2(1), 13. doi:10.1007/s41062-017-0064-9.

[12] Ghorbani, A., Hasanzadehshooiili, H., Somti Foumani, M. A., Medzvieckas, J., & Kliukas, R. (2023). Liquefaction Potential of Saturated Sand Reinforced by Cement-Grouted Micropiles: An Evolutionary Approach Based on Shaking Table Tests. Materials, 16(6), 2194. doi:10.3390/ma16062194.

[13] Ou Yang, F., Fan, G., Wang, K., Yang, C., Lyu, W., & Zhang, J. (2021). A large-scale shaking table model test for acceleration and deformation response of geosynthetic encased stone column composite ground. Geotextiles and Geomembranes, 49(5), 1407–1418. doi:10.1016/j.geotexmem.2021.05.013.

[14] Shanmugam, G. K., Godson, M. D., Yogesh, R. V., Jeeva, S. K., & Madhiyarasu, P. (2023). Experimental Observations on In-Situ Ground Response During Sequential Installation of Stone Column Improvement in the Saturated Ground. International Journal of Geosynthetics and Ground Engineering, 9(6), 69. doi:10.1007/s40891-023-00489-0.

[15] Bayati, H., & Bagheripour, M. H. (2019). Shaking table study on liquefaction behaviour of different saturated sands reinforced by stone columns. Marine Georesources and Geotechnology, 37(7), 801–815. doi:10.1080/1064119X.2018.1492051.

[16] Diana, N. A., Soemitro, R. A. A., Ekaputri, J. J., Satrya, T. R., & Warnana, D. D. (2025). Dynamic Analysis of MICP-Stabilized Soil and Liquefiable Soil With Varying Salinity Levels. Civil Engineering Journal, 11(4), 1432–1446. doi:10.28991/CEJ-2025-011-04-010.

[17] Padmanabhan, G., & Shanmugam, G. K. (2021). Liquefaction and reliquefaction resistance of saturated sand deposits treated with sand compaction piles. Bulletin of Earthquake Engineering, 19(11), 4235–4259. doi:10.1007/s10518-021-01143-8.

[18] Zhu, Z., Zhou, Y., Han, K., Wu, H., & Zhao, S. (2022). Liquefaction and Reliquefaction Characteristics of Aeolian Sand Foundation Reinforced by Precast Cement Piles Based on Shaking Table Test. Geofluids, 5344230. doi:10.1155/2022/5344230.

[19] Yoon, J. C., Son, S. W., & Kim, J. M. (2024). Comparison of Liquefaction Damage Reduction Performance of Sheet Pile and Grouting Method Applicable to Existing Structures Using 1-G Shaking Table. Buildings, 14(9), 2676. doi:10.3390/buildings14092676.

[20] Suyadil, Harianto, T., Muhiddin, A. B., & Arsyad, A. (2023). Soil Reinforcement Model Test Using Timber Pile at Liquefaction Area. Civil Engineering Journal (Iran), 9(6), 1509–1521. doi:10.28991/CEJ-2023-09-06-016.

[21] Maheshwari, B. K., & Padmanabhan, G. (2025). Liquefaction and reliquefaction mitigation of sand specimen treated with prefabricated vertical drains: An experimental investigation. Geotextiles and Geomembranes, 53(1), 295–310. doi:10.1016/j.geotexmem.2024.09.018.

[22] Padmanabhan, G., & Shanmugam, G.K. (2025). Effect of Drainage and Densification Mechanism in Mitigating Liquefaction During Repeated Shaking Events. Soil Dynamics and Computational Geomechanics. IYGEC 2021. Lecture Notes in Civil Engineering, Springer, Singapore. doi:10.1007/978-981-96-1368-7_7.

[23] Ghassemi, S., Ekraminia, S. S., Hajialilue-Bonab, M., Tohidvand, H. R., Azarafza, M., & Derakhshani, R. (2025). Innovative insights into micropile seismic response: Shaking table tests reveal critical dependencies and liquefaction mitigation. Bulletin of Engineering Geology and the Environment, 84(4), 206. doi:10.1007/s10064-025-04225-y.

[24] Yogesh, R. V., Ganesh Kumar, S., & Santha Kumar, G. (2026). Synergetic effect of densification, drainage and shear reinforcement mechanism of sustainable pervious concrete pile for liquefaction and reliquefaction mitigation. Soil Dynamics and Earthquake Engineering, 200, 109842. doi:10.1016/j.soildyn.2025.109842.

[25] ASTM D4253-16e1. (2025). Standard Test Methods for Maximum Index Density and Unit Weight of Soils Using a Vibratory Table. ASTM International, Pennsylvania, United States.

[26] ASTM D4254-16. (2025). Standard Test Methods for Minimum Index Density and Unit Weight of Soils and Calculation of Relative Density. ASTM International, Pennsylvania, United States.

[27] Lombardi, D., & Bhattacharya, S. (2012). Shaking table tests on rigid soil container with absorbing boundaries. Proceedings of the 15th World Conference on Earthquake Engineering (15 WCEE), 24-28 September, 2012, Lisbon, Portugal.

[28] Lombardi, D., Bhattacharya, S., Scarpa, F., & Bianchi, M. (2015). Dynamic response of a geotechnical rigid model container with absorbing boundaries. Soil Dynamics and Earthquake Engineering, 69, 46–56. doi:10.1016/j.soildyn.2014.09.008.

[29] ASTM D5311-11. (2012). Standard Test Method for Load Controlled Cyclic Triaxial Strength of Soil. ASTM International, Pennsylvania, United States. doi:10.1520/D5311-11.

[30] GS 0541-2020. (2020). Method for cyclic undrained triaxial test on soils. Japanese Geotechnical Society Standard, Bunkyo-ku, Japan.

[31] Bharathi, M., Dubey, R. N., & Shukla, S. K. (2019). Experimental investigation of vertical and batter pile groups subjected to dynamic loads. Soil Dynamics and Earthquake Engineering, 116, 107–119. doi:10.1016/j.soildyn.2018.10.012.

[32] Li, W. W., Chen, Y. M., Liu, H. L., Yang, Y. H., & Zhang, X. L. (2018). Shaking table tests on efficiency of improvement of X-section piles against lateral spreading. Yantu Gongcheng Xuebao/Chinese Journal of Geotechnical Engineering, 40(5), 945–952. doi:10.11779/CJGE201805021.

[33] ASTM D3441-05. (2016). Standard Test Method for Mechanical Cone Penetration Tests of Soil. ASTM International. doi:10.1520/D3441-05.

[34] Jamiolkowski, M., Lo Presti, D. C. F., & Manassero, M. (2003). Evaluation of Relative Density and Shear Strength of Sands from CPT and DMT. Soil Behavior and Soft Ground Construction, 201–238. doi:10.1061/40659(2003)7.

[35] Robertson, P. K. (2016). Cone penetration test (CPT)-based soil behaviour type (SBT) classification system — An update. Canadian Geotechnical Journal, 53(12), 1910–1927. doi:10.1139/cgj-2016-0044.

[36] García-Torres, S., & Madabhushi, G. S. P. (2019). Performance of vertical drains in liquefaction mitigation under structures. Bulletin of Earthquake Engineering, 17(11), 5849–5866. doi:10.1007/s10518-019-00717-x.

[37] Iai, S. (1989). Similitude for Shaking Table Tests on Soil-Structure-Fluid Model in 1g Gravitational Field. Soils and Foundations, 29(1), 105–118. doi:10.3208/sandf1972.29.105.